processes

Article

Development for Cooling Operations through a Model of Nanofluid Flow with Variable Heat Flux and Thermal Radiation

Mohammed Alrehili

Department of Mechanical Engineering, Faculty of Engineering, University of Tabuk, Tabuk 71491, Saudi Arabia; malrehili@ut.edu.sa

Abstract: This article discusses the flow of a non-Newtonian Carreau nanoliquid across a stretching radiative nonlinear sheet that is exposed to a variable heat flux. Analysis is done with changing thermal conductivity since it affects how heat and mass transfer occur. Nanoparticles are modelled using the Brownian motion and the thermophoresis phenomenon. The introduction of a similar solution to our challenge, as obtained by our paper, received significant attention. To create a dimensionless system, the governing partial differential equations are subjected to the mathematical model's convenient similarity transformations after it has been developed. The numerical solution of the coupled highly nonlinear ordinary differential equations characterizing velocity, temperature and nanoparticles concentration is shown using an effective shooting approach. Additionally, all factors affecting the situation that could increase the effectiveness of cooling operations will be looked into. Results for velocity, the thermal field, the concentration of nanoparticles, the skin-friction coefficient, and the local Nusselt and Sherwood numbers are provided and explored. Tables and graphics will be used to illustrate the paper's conclusions. Results are also given in comparison to existing literature. Excellent agreement has been reached. Furthermore, it is clear that the local Sherwood number, the local Nusselt number, and the skin friction coefficient are all observed to increase as the power law index does.

Keywords: variable heat flux; non-newtonian nanofluid; variable conductivity; thermal radiation; non-linear stretching sheet; viscous dissipation

Citation: Alrehili, M. Development for Cooling Operations through a Model of Nanofluid Flow with Variable Heat Flux and Thermal Radiation. *Processes* **2022**, *10*, 2650. https://doi.org/10.3390/pr10122650

Academic Editor: Blaž Likozar

Received: 26 November 2022
Accepted: 7 December 2022
Published: 9 December 2022

1. Introduction

Because of its major impact on a number of technological processes, a significant amount of attention has been given over the past few decades to a crucial type of fluid called the non-Newtonian fluid over a stretching surface. Numerous non-Newtonian liquids are being used more often in engineering and industry, including liquid metals, nuclear fuel slurries, mercury amalgams, plastic films, biological fluids, synthetic fibres, paper coatings, and lubricating oils. Models of the behavior of diluted polymeric fluids and biological fluids have been developed using non-Newtonian fluids of the differential types with great success. The polymer industry has significant uses for the flow of an incompressible viscous fluid over a stretched surface. For example, a variety of technological procedures using polymers entail pulling continuous filaments (or strips) that have been ejected from a die through a liquid with a regulated cooling system, stretching the strips occasionally while they do so. Likewise, the amount of heat transferred at the stretching sheet determines a majority of the final product's quality. Crane [1] was a pioneer scientist in the area of fluid flow caused by a stretching sheet who discovered an exact and precise solution to the fluid flow problem. Several non-Newtonian models, including the viscoelastic model [2], the power-law model [3,4], the Sisko model [5,6], the Maxwell model [7,8], the Williamson model [9,10], and the micropolar model [11,12], are particularly important and can be used in engineering applications and industry. Another crucial and essential category of rate type non-Newtonian fluids is the Carreau model which first came up by Carreau [13]. The non-Newtonian Carreau model reveals a fundamental link between low shear rates and greater shear rates. Since then, a large number of scientists [14–16] have looked into the behavior of the Carreau fluid in diverse morphologies.

When designing very sophisticated energy conversion systems that operate at high temperatures, consideration of the effects of thermal radiation on flow and heat transfer mechanisms is crucial. In the polymer processing industry, where the quality of the finished product depends in part on the variables regulating heat transport, thermal radiation impact may be a significant factor. When there is a notable change between surface temperature and ambient temperature, thermal radiation impacts become significant. Additionally, the effect of thermal radiation on non-Newtonian fluid flow is crucial, particularly in the fields of nuclear power, solar energy, aircraft propulsion, and chemical processes at high operating temperatures. The relevance of the thermal radiation phenomenon and its effects on the Carreau fluid flow have led numerous scientists to explore a variety of problems in this area [16–18].

In an ordinary heat transfer fluid, nanoparticles are suspended, creating a nanofluid for heat transfer. A nanofluid is created when a common base fluid is mixed with nanoparticles no larger than 100 nm. Colloid suspensions make up nanofluids. Compared to fluids dispersed with micron-sized particles, a nanofluid may have a higher viscosity because of the rise in effective volume fraction caused by the electrical double layer surrounding the particles. Additionally, nanofluids have a variety of useful applications in industry research as well as in the real world, such as the use of nanofluids as a cooling medium in nuclear systems and the development of highly efficient nano-drugs for the treatment of a wide range of diseases. Choi [19] has presented his ground breaking work, which mainly focused on the thermal characteristics of nanofluid flow. Following Choi's scientific breakthrough, Buongiorno [20] has discussed the topic of improving heat transmission by analysing nanofluid flow. Given the importance of the nanofluid flow, especially with Carreau models, numerous scholars focus on a variety of non-Newtonian Carreau nanofluid flow problems [21–26].

Because non-Newtonian nanofluids are noteworthy, the flow of a Carreau nanofluid caused by a nonlinearly stretching sheet with viscous dissipation phenomenon has been taken into consideration. Nanofluid flow resulting from stretching a surface with thermal radiation. Further consideration is given to nanofluid thermal conductivity that is temperature-dependent. On the sheet surface, variable heat flux phenomenon is invoked. Due to the random movement of nanoparticles, Brownian motion and thermophoresis are taken into consideration when explaining the characteristics of nanoparticles. By using the shooting approach, the governing equations for the Carreau nanofluid with changing heat flow are developed. The velocity distribution, temperature profile, and concentration profile are represented graphically in the results.

2. Flow Analysis

Here, in Figure 1 in the plane xy, we examine the two-dimensional flow of a non-Newtonian, incompressible Carreau nanofluid that characterized by the time constant Γ over an impermeable stretched surface that is susceptible to a heat flux q_w. Within the domain $y > 0$, the flow of nanofluid is restrained. Here, we have the Cartesian coordinates so that the $x-$axis runs parallel to the stretching surface and the $y-$axis runs perpendicular to the sheet. Assume that the components of the nanofluid velocity in the x, and y directions be u and v, respectively.

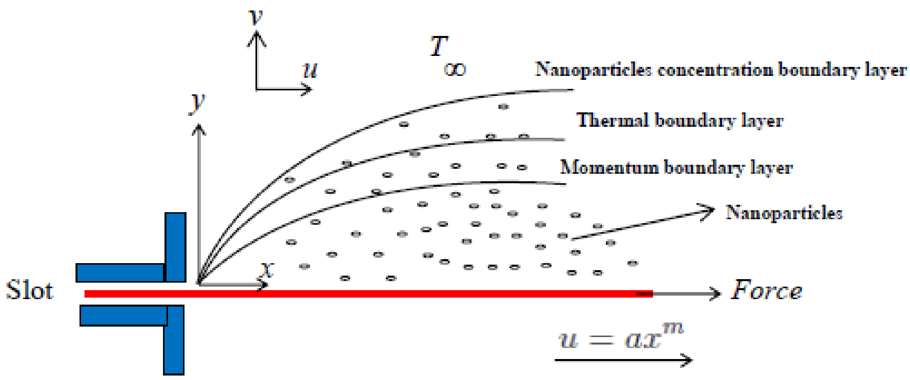

Figure 1. Sketch of flow geometry.

Throughout this study, it is anticipated that the elastic sheet will be subject to a force that controls the fluid's velocity by the equation [27]:

$$u = ax^m, \tag{1}$$

where the stretching is exemplified by the parameter m and a is a positive constant. Also, the motion of nanofluid is presumptively subject to a radiative heat flux q_r that can be controlled by the following equation [27]:

$$q_r = -\frac{4\sigma^*}{3k^*}\frac{\partial T^4}{\partial y}, \tag{2}$$

where σ^* is the Stefan-Boltzmann constant and k^* is the coefficient of absorption. Here, it is important to note that the Rosseland approximation is used in the last equation to represent the radiative heat flux in order to avoid the non-linear nature of the radiation term. Also, in order for T^4 to be expanded in a Taylor series, it is presumable that the temperature variation within the flow is quite tiny according to the following relation [27]:

$$T^4 \cong 4T_\infty^3 T - 3T_\infty^4. \tag{3}$$

Further, the Brownian motion of the nanoparticles and the thermophoresis phenomenon are taken into account. Additionally, The base fluid's Brownian diffusion coefficient D_B is used to model the nanoparticles' motion, which is believed to be random. On the other hand, in accordance with the thermophoresis diffusion coefficient D_T, it is expected that nanoparticles are thermally dispersed. The concentration of the nanoparticles in the nanofluid is symbolized by C, whereas the concentration of nanoparticles near the sheet is assumed to governed by:

$$C_w(x) = C_\infty + Bx^{2m}, \tag{4}$$

where C_∞ is the ambient nanoparticles concentration and B is a constant. The governing equations in the presence of thermal radiation and viscous dissipation are now provided by under the presumptions made previously, in terms of velocity components, temperature, and concentration [27] as follows:

$$\frac{\partial u}{\partial x} + \frac{\partial v}{\partial y} = 0, \tag{5}$$

$$u\frac{\partial u}{\partial x} + v\frac{\partial u}{\partial y} = \frac{\mu}{\rho}\frac{\partial}{\partial y}\left(\frac{\partial u}{\partial y}\left(1 + \Gamma^2\left(\frac{\partial u}{\partial y}\right)^2\right)^{\frac{n-1}{2}}\right), \tag{6}$$

$$u\frac{\partial T}{\partial x}+v\frac{\partial T}{\partial y}=\frac{1}{\rho c_p}\frac{\partial}{\partial y}\left(\kappa(T)\frac{\partial T}{\partial y}\right)+\frac{\mu}{\rho c_p}\left(\frac{\partial u}{\partial y}\right)^2\left(1+\Gamma^2\left(\frac{\partial u}{\partial y}\right)^2\right)^{\frac{n-1}{2}}-\frac{1}{\rho c_p}\frac{\partial q_r}{\partial y}+\tau\left(D_B\frac{\partial C}{\partial y}\frac{\partial T}{\partial y}+\frac{D_T}{T_\infty}\left(\frac{\partial T}{\partial y}\right)^2\right), \tag{7}$$

$$u\frac{\partial C}{\partial x}+v\frac{\partial C}{\partial y}=D_B\frac{\partial^2 C}{\partial y^2}+\frac{D_T}{T_\infty}\frac{\partial^2 T}{\partial y^2}, \tag{8}$$

where ρ being the nanofluid density, c_p is the specific heat at constant pressure, T_∞ is the ambient temperature and n is the power law index. It is important to note that our prior non-Newtonian Carreau model can be converted into a Newtonian model when $n=1$. Additionally, the following are the boundary conditions for these earlier governing equations [27]:

$$u=ax^m,\quad C=C_w,\quad v=0,\quad -\kappa_{eff}\frac{\partial T}{\partial y}=q_w=Ax^r,\quad at\quad y=0, \tag{9}$$

$$u\to 0,\quad T\to T_\infty,\quad C\to C_\infty \text{ as } y\to\infty, \tag{10}$$

where κ_{eff} is the effective thermal conductivity which can be described as follows based on the existence of thermal radiation [27]:

$$\kappa_{eff}=\kappa(T)+\frac{16\sigma^* T_\infty^3}{3k^*}. \tag{11}$$

As a result of the final expression, the energy Equation (7) can be expressed as follows:

$$u\frac{\partial T}{\partial x}+v\frac{\partial T}{\partial y}=\frac{1}{\rho c_p}\frac{\partial}{\partial y}\left(\kappa_{eff}\frac{\partial T}{\partial y}\right)+\frac{\mu}{\rho c_p}\left(\frac{\partial u}{\partial y}\right)^2\left(1+\Gamma^2\left(\frac{\partial u}{\partial y}\right)^2\right)^{\frac{n-1}{2}}+\tau\left(D_B\frac{\partial C}{\partial y}\frac{\partial T}{\partial y}+\frac{D_T}{T_\infty}\left(\frac{\partial T}{\partial y}\right)^2\right). \tag{12}$$

Now, the following dimensionless variables [27] are introduced in order to look for similarity solutions for the governing Equations (5)–(8) subject to boundary conditions (9) and (10):

$$\eta=\sqrt{\frac{\rho a(m+1)}{2\mu}}x^{\frac{m-1}{2}}y,\qquad \psi(x,y)=\sqrt{\frac{2\mu a}{\rho(m+1)}}x^{\frac{m+1}{2}}f(\eta), \tag{13}$$

$$T=T_\infty+\frac{A}{\kappa_\infty}\sqrt{\frac{2\mu}{\rho a(m+1)}}x^{\frac{2r-m+1}{2}}\theta(\eta),\quad \phi(\eta)=\frac{C-C_\infty}{C_w-C_\infty}, \tag{14}$$

where η is the dimensionless variable, f is the non-dimensional stream function, θ is the non-dimensional fluid temperature and ϕ is the dimensionless concentration. Likewise, the following relationship is used to take into account the fundamental relationship between the nanofluid thermal conductivity $\kappa(T)$ and the dimensionless temperature θ [28]:

$$\kappa(T)=\kappa_\infty(1+\varepsilon\theta), \tag{15}$$

where ε is the thermal conductivity parameter and κ_∞ is the ambient thermal conductivity. by considering the supposition of thermal conductivity and after utilizing the aforementioned dimensionless transformations (13) and (14), the equation for continuity Equation (5) is quickly and easily satisfied, whereas the remaining fundamental equations are reduced as follows:

$$\left(1+W_e^2 f''^2\right)^{\frac{n-3}{2}}\left[\left(1+nW_e^2 f''^2\right)f'''\right]-\left(\frac{2m}{m+1}\right)f'^2+ff''=0, \tag{16}$$

$$\frac{1}{Pr}\left(\varepsilon\theta'^2+(1+R+\varepsilon\theta)\theta''\right)+\left(f\theta'+\left(\frac{m-2r-1}{m+1}\right)f'\theta\right)+Nt\theta'^2+Nb\theta'\phi'+ Ecf''^2\left(1+W_e^2 f''^2\right)^{\frac{n-1}{2}}=0, \tag{17}$$

$$\phi''+\mathrm{PrLe}\left(f\phi'-\frac{4m}{m+1}\phi f'\right)+\frac{Nt}{Nb}\theta''=0. \tag{18}$$

Accordingly, the modified boundary conditions are as follows:

$$f=0,\quad f'=1,\quad \phi=1,\quad \theta'(0)=\frac{-1}{1+R+\varepsilon\theta(0)},\quad at\quad \eta=0, \tag{19}$$

$$f'\to 0,\quad \theta\to 0,\quad \phi\to 0,\quad \text{as } \eta\to\infty. \tag{20}$$

The following definitions for each of the parameters that control the momentum, energy, and concentration equations are given:

$$Nb=\frac{\tau D_B\rho(C_w-C_\infty)}{\mu}, W_e=\left(\frac{\rho a^3(m+1)\Gamma^2 x^{3m-1}}{2\mu}\right)^{\frac{1}{2}}, R=\frac{16\sigma^* T_\infty^3}{3\kappa_\infty k^*}, \Pr=\frac{\mu c_p}{\kappa_\infty}, \tag{21}$$

$$Nt=\frac{\tau D_T\rho\left(\frac{A}{\kappa_\infty}\sqrt{\frac{2\mu}{\rho a(m+1)}}x^{\frac{2r-m+1}{2}}\right)}{\mu T_\infty}, Ec=\frac{u_w^2}{c_p\left(\frac{A}{\kappa_\infty}\sqrt{\frac{2\mu}{\rho a(m+1)}}x^{\frac{2r-m+1}{2}}\right)}, Le=\frac{\kappa_\infty}{\rho c_p D_B}, \tag{22}$$

which accordingly, indicates the Brownian motion parameter Nb, the local Weissenberg number W_e, the radiation parameter R, the Prandtl number Pr, the thermophoresis parameter Nt, the Eckert number Ec and the Lewis number Le.

3. Applicable Quantities in Engineering and Industry

The physical parameters of the Carreau nanofluid flow based on the variable heat flux that are significant to engineering and industry in the processing of materials are the skin-friction coefficient Cf_x, heat transfer coefficient Nux, and mass transfer coefficient Shx, and they can be identified as follows:

$$Re_x^{\frac{1}{2}}Cf_x=-2\sqrt{\frac{m+1}{2}}\left[1+W_e^2\left(f''(0)\right)^2\right]^{\frac{n-1}{2}}f''(0), \tag{23}$$

$$Re_x^{\frac{-1}{2}}Nu_x=\frac{\sqrt{\frac{m+1}{2}}}{\theta(0)},\quad Re_x^{\frac{-1}{2}}Sh_x=-\sqrt{\frac{m+1}{2}}\phi'(0), \tag{24}$$

where $Re_x=\frac{u_w x}{\nu}$ is the local Reynolds number.

4. Validation of the Numerical Solution

The fourth-order Runge-Kutta method combined with the shooting technique is used here to solve the non-dimensional governing Equations (16) through (18) and their associated boundary conditions (19) and (20). To ensure the efficacy and correctness of the current analysis, findings on the skin-friction coefficient in terms of $-f''(0)$ were compared with Cortell's stated results for Newtonian case $n=1$ over a nonlinearly stretching sheet with different values of the stretching parameter m and in the absence of the local Weissenberg number $W_e=0$. Table 1 demonstrates that there is excellent agreement between the comparisons in the aforementioned cases. After this positive assessment of our numerical strategy, we will discuss the numerical results for the Carreau nanofluid model that was impacted by the variable heat flux.

Table 1. Comparison values of $-f''(0)$ for various values of m with $n = 1.0$ and $W_e = 0.0$.

m	Cortell [29]	Present Study
0.1	0.705897	0.705896891
0.3	0.815696	0.8156951478
0.6	0.918172	0.9181715984
0.9	0.983242	0.9832417810
1.0	1.000000	1.0000000000
1.5	1.061587	1.0615865590
3.0	1.148588	1.1485877582
10.0	1.234875	1.2348748792

5. Interpretation of Numerical Results

This study examines the problem of flow and heat mass transfer in a viscous non-Newtonian Carreau nanofluid across a stretching surface that is nonlinearly stretched in the influence of viscous dissipation and thermal radiation. The radiative heat flux is approximated using the Rosseland approximation. We look at how the relevant parameters, including the power-law index parameter n, the local Weissenberg number W_e, the radiation parameter R, the thermal conductivity parameter ε, the Prandtl number Pr, the thermophoresis parameter Nt, the Eckert number Ec, and the Lewis number Le, affect the velocity $f'(\eta)$, temperature $\theta(\eta)$, and concentration $\phi(\eta)$ profiles in order to obtain a comprehensive physical understanding of the problem. Figure 2 depicts how the power law index n affects the velocity, temperature, and concentration curves. The boundary layer tends to become thicker with higher values of the power law index, which causes the velocity distribution $f'(\eta)$ through the boundary layer to grow. Additionally, Figure 2b shows that as the power law index rises, the temperature $\theta(\eta)$ and concentration $\phi(\eta)$ of nanofluids both fall. Because the sheet temperature $\theta(0)$ is lowered as n rises due to the existence of heat flux in our research, the power law index acts as a coolant factor for the stretching sheet. Furthermore , Khan and Hashim's earlier work [30] produced results for the power law index parameter that were consistent with our current findings.

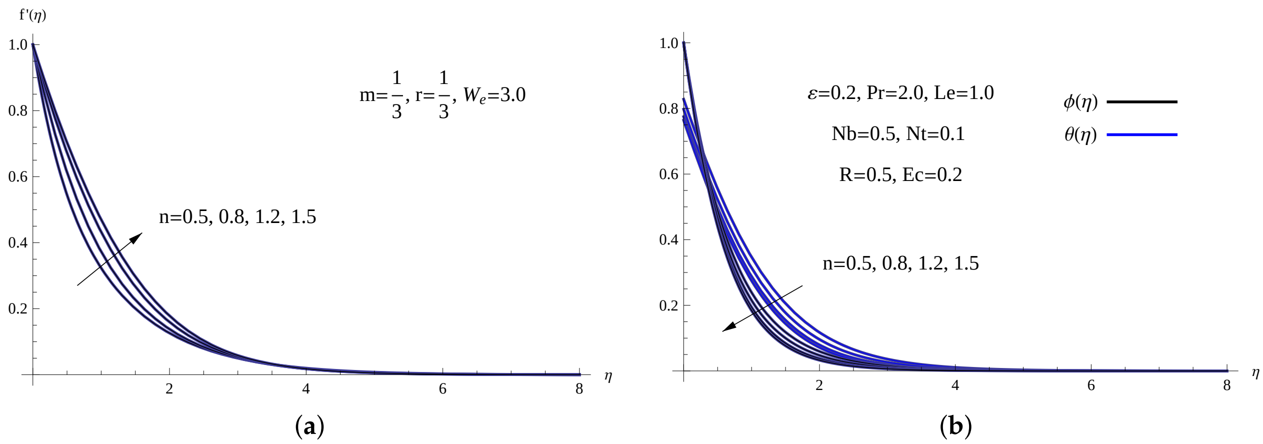

Figure 2. (**a**) $f'(\eta)$ via n; (**b**) $\theta(\eta)$ and $\phi(\eta)$ via n.

With the variation of the local Weissenberg number W_e, Figure 3 plots the velocity, temperature, and concentration fields. The velocity field is seen to diminish as the local Weissenberg number does, although the temperature and concentration fields have the opposite impact for the same parameter. Additionally, the same figure shows that a thinner boundary layer is caused by a high value of the local Weissenberg number. Physically, as the Weissenberg number increases, so does the resistance to fluid motion. Additionally, identical outcomes involving the same local Weissenberg number were obtained on both the momentum and temperature fields in Megahed's earlier work [27], supporting our current findings.

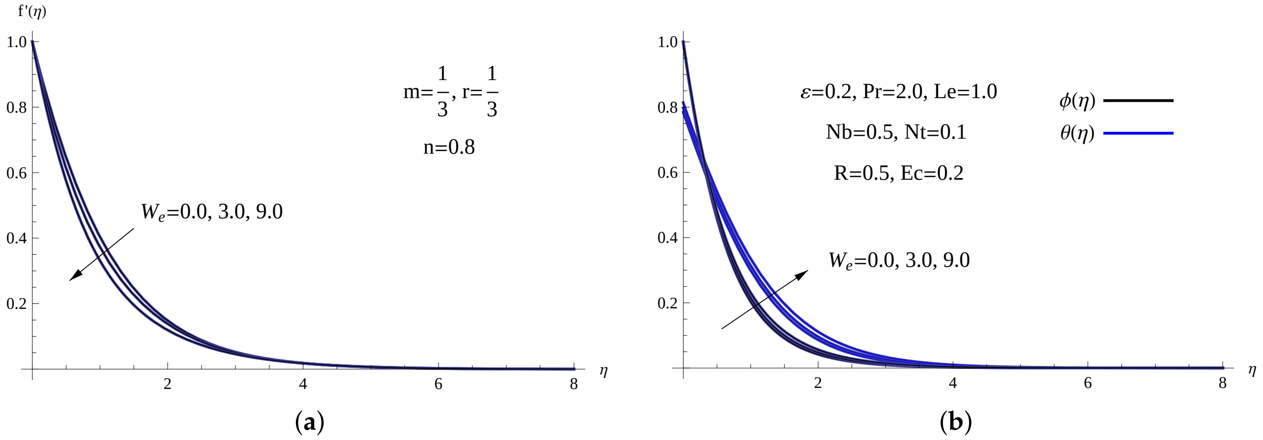

Figure 3. (**a**) $f'(\eta)$ via W_e; (**b**) $\theta(\eta)$ and $\phi(\eta)$ via W_e.

In Figure 4, for various values of the radiation parameter R, temperature $\theta(\eta)$ and concentration $\phi(\eta)$ profiles throughout the boundary layer with variable heat flux are shown. This figure shows, as anticipated, that both the temperature profiles $\theta(\eta)$ along the sheet and the sheet temperature $\theta(0)$ demonstrate a decreasing behavior as the radiation parameter R rises, whereas the inverse correlation is seen away from the sheet for the temperature profiles $\theta(\eta)$. Since k^* reduces as the divergence of the radiative heat flux $\frac{\partial q_r}{\partial y}$ grows, the rate of radiative heat transfer to the fluid also increases, raising the fluid's temperature. So, the thickening of the thermal boundary layer is caused by the radiation parameter R. In terms of physics, this allows the fluid to escape the heat energy from the flow zone and cools the system. Further, we notice that the radiation parameter has a minimal impact on the concentration profiles across the whole boundary layer since it indirectly influences the concentration field. Moreover, the pioneering work of Megahed [27], which supports our present findings, shows that the radiation parameter has the same impact on the thermal field when heat flux is present.

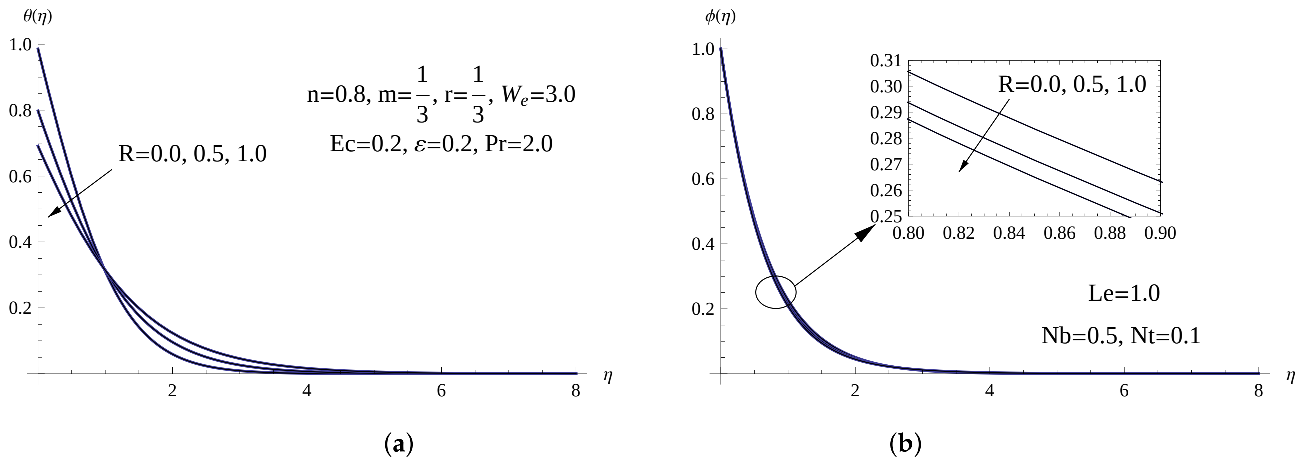

Figure 4. (**a**) $\theta(\eta)$ via R; (**b**) $\phi(\eta)$ via R.

Figure 5 displays a temperature $\theta(\eta)$ and concentration $\phi(\eta)$ impact graph for various values of the thermal conductivity parameter ε. When the thermal conductivity parameter's values increase, the nanofluid temperature distribution slows down, particularly close to the sheet, while the opposite scenario occurs away from the sheet, thickening the thermal boundary layer. In light of this, systems, especially those with variable heat flux, may choose to use the thermal conductivity parameter as a coolant parameter. The concentration field is indirectly impacted by the thermal conductivity parameter, thus as it grows, the concentration of nanoparticles somewhat declines.

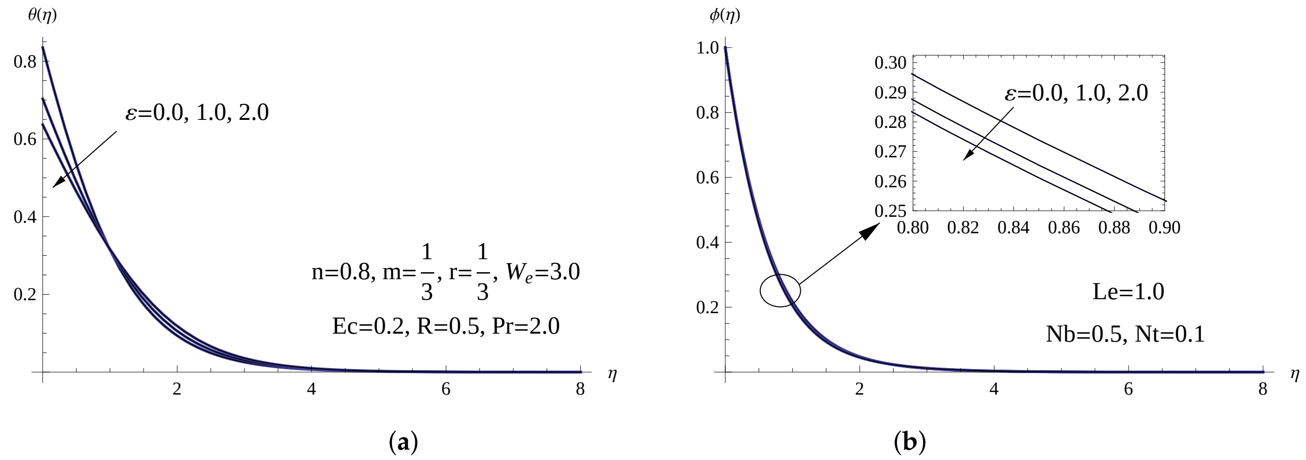

Figure 5. (**a**) $\theta(\eta)$ via ε; (**b**) $\phi(\eta)$ via ε.

Figure 6 displays a graph illustrating the relationship between temperature $\theta(\eta)$ and the concentration $\phi(\eta)$ of nanoparticles as the Eckert number Ec varies. The graph of nanoparticle concentration increases slightly with increasing Eckert number value, as does the temperature of the nanofluid but with a significantly variance behavior. If we look at Megahed's earlier published work [27] on the Eckert number, the current results are also supported by it.

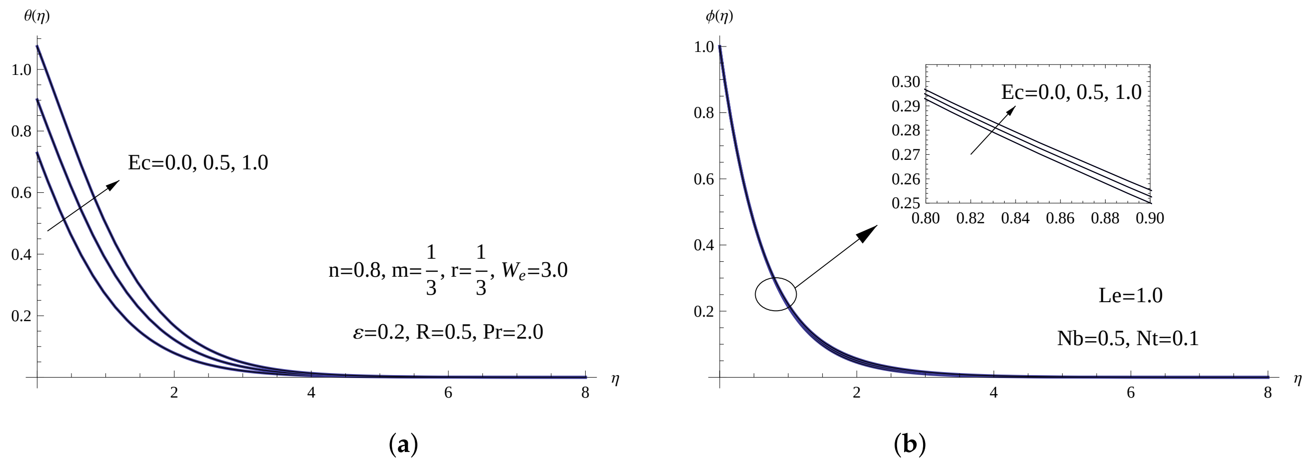

Figure 6. (**a**) $\theta(\eta)$ via Ec; (**b**) $\phi(\eta)$ via Ec.

Temperature $\theta(\eta)$ and concentration $\phi(\eta)$ distribution are depicted in Figure 7 together with the thermophoresis parameter's Nt variation. In the temperature profile, the thermophoresis parameter marginally improved the temperature distribution compared to the nanoparticle concentration distribution. This behavior will assist to thicken the thermal boundary layer and raise the sheet temperature $\theta(0)$. The thermophoresis phenomenon, in terms of its physical meaning, entails the evacuation of warmed particles from a heated surface and their transport to a cool environment. As a result, the fluid's temperature goes up.

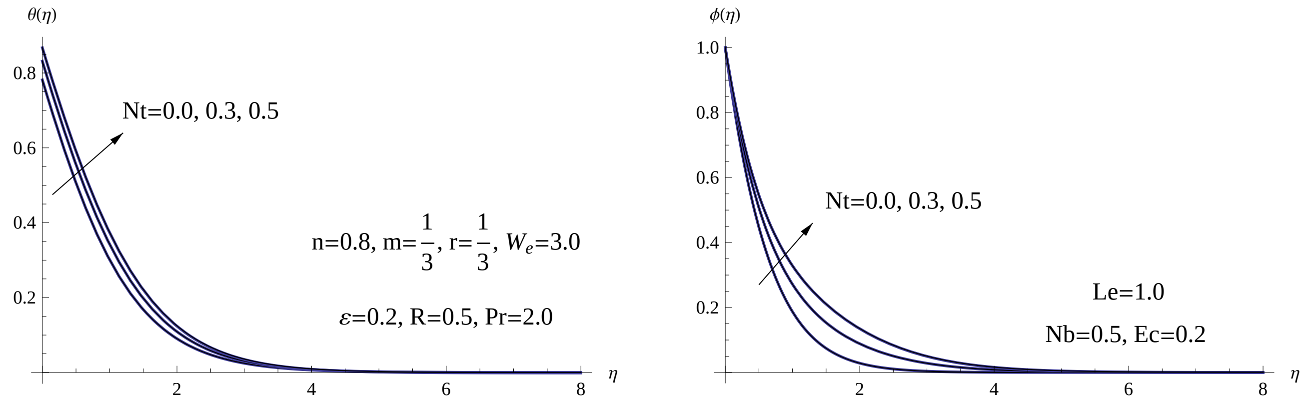

(**a**) (**b**)

Figure 7. (**a**) $\theta(\eta)$ via Nt; (**b**) $\phi(\eta)$ via Nt.

Figure 8 shows how the Brownian motion parameter Nb affects thermal behavior and mass diffusion of nanoparticles. Because of the nature of the Brownian motion parameter, raising it causes the nanoparticles to move randomly more often, which lowers the concentration $\phi(\eta)$ of the nanofluid as observed. Additionally, it is implied that the temperature profile near the stretching sheet area tends to significantly boost as Nb increases. According to the definition of Brownian motion, rising Nb results from the sparsity of the fluid's viscosity. As a result, the kinetic energy of the nanoparticles is enhanced by the erratic flow movement, which raises the temperature of the Carreau nanofluid. Furthermore, the results of earlier research by Alrihieli et al. [31] regarding the Brownian motion parameter support our current findings.

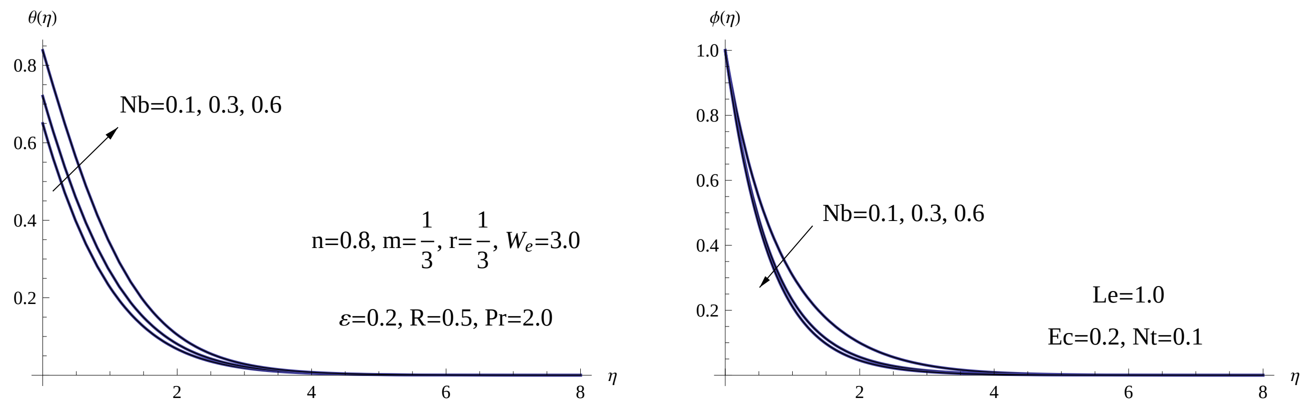

(**a**) (**b**)

Figure 8. (**a**) $\theta(\eta)$ via Nb; (**b**) $\phi(\eta)$ via Nb.

Figure 9 provides an illustration of the impact of the Prandtl number Pr on the thermal field $\theta(\eta)$ and the mass diffusion of nanoparticles $\phi(\eta)$. According to the meaning of the Prandtl number, boosting its magnitude indicates either an increase in nanofluid viscosity or a decrease in flow thermal diffusivity; as a consequence, both the sheet temperature $\theta(0)$ and the thickness of the thermal boundary layer falls as the Prandtl number enhances. Additionally, the Prandtl number makes it easy to see how the concentration of nanoparticles has decreased.

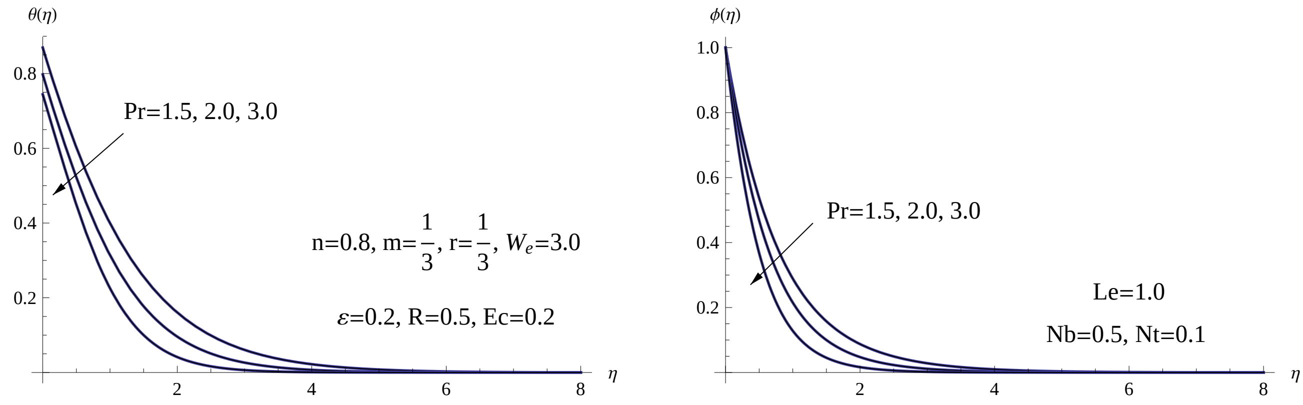

(**a**) (**b**)

Figure 9. (**a**) $\theta(\eta)$ via Pr; (**b**) $\phi(\eta)$ via Pr.

Figure 10 illustrates how the Lewis number Le affects the temperature $\theta(\eta)$ and concentration $\phi(\eta)$ curves. This figure shows that as the Lewis number Le grows, both the sheet temperature $\theta(0)$ and the temperature $\theta(\eta)$ of nanofluids moving through the thermal layer somewhat increase, and as a result, the thickness of the thermal boundary layer also slightly increases. Additionally, this graph elucidate that as the Lewis number increases, the molecular diffusivity drops, which leads to a fall in the nanofluid concentration.

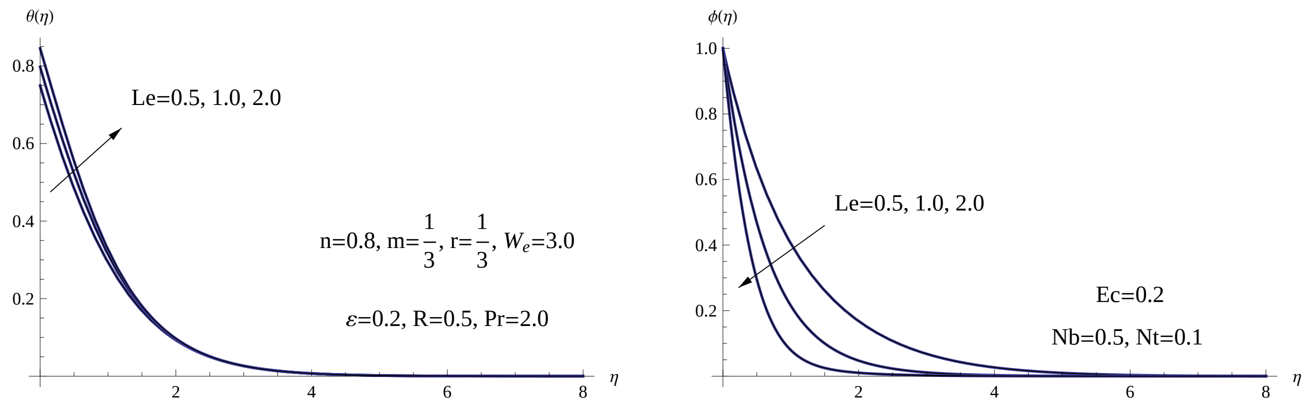

(**a**) (**b**)

Figure 10. (**a**) $\theta(\eta)$ via Le; (**b**) $\phi(\eta)$ via Le.

Now, in Table 2 an review of all the governing factors and how they affect the suggested model reveals that, for high values of the radiation parameter, thermal conductivity parameter, and power law index, the cooling process that is hoped to be reached in more industrial processes can be attained. Additionally, to fulfill the priceless explanation of every physical phenomenon that results from the flow and mass transfer of non-Newtonian Carreau nanofluid. The following table is designed to outline the anticipated behaviour that may arise from the influence of controlling factors on the local skin-friction coefficient $Re_x^{\frac{1}{2}} Cf_x$, the local Nusselt number $Re_x^{\frac{-1}{2}}\, Nu_x$, and the local Sherwood number $Re_x^{\frac{-1}{2}}\, Sh_x$. The local skin-friction coefficient, the local Nusselt number, and the local Sherwood number all rise naturally as the power law index improves, but they all decrease as the local Weissenberg number rises. It should be noted that higher values of the thermal conductivity and radiation parameters both lead to increases in the local Nusselt number and local Sherwood number findings. Further, it is observed that whereas increasing values of the thermophoresis parameter exhibit the opposite tendency, both the local Nusselt number and the local Sherwood number rise with the superior growth in the Prandtl number.

Furthermore, the Lewis number greatly improved the local Sherwood number, whereas the local Nusselt number behaved in the opposite manner.

Table 2. Values of $Re_x^{\frac{1}{2}} Cf_x$, $Re_x^{\frac{-1}{2}} Nu_x$ and $Re_x^{\frac{-1}{2}} Sh_x$ for various values of $n, \varepsilon, W_e, Ec, R, Nb, Pr, Le$ and Nt with $m = \frac{1}{3}$ and $r = \frac{1}{3}$.

n	W_e	R	ε	Ec	Nt	Nb	Pr	Le	$Re_x^{\frac{1}{2}} Cf_x$	$Re_x^{\frac{-1}{2}} Nu_x$	$Re_x^{\frac{-1}{2}} Sh_x$
0.5	3.0	0.5	0.2	0.2	0.1	0.5	2.0	1.0	1.05719	0.986153	1.15776
0.8	3.0	0.5	0.2	0.2	0.1	0.5	2.0	1.0	1.24664	1.023721	1.20708
1.2	3.0	0.5	0.2	0.2	0.1	0.5	2.0	1.0	1.45421	1.053810	1.24654
1.5	3.0	0.5	0.2	0.2	0.1	0.5	2.0	1.0	1.58807	1.068621	1.26604
0.8	0.0	0.5	0.2	0.2	0.1	0.5	2.0	1.0	1.35541	1.040711	1.22935
0.8	3.0	0.5	0.2	0.2	0.1	0.5	2.0	1.0	1.24664	1.023721	1.20708
0.8	9.0	0.5	0.2	0.2	0.1	0.5	2.0	1.0	1.11824	1.003390	1.17883
0.8	3.0	0.0	0.2	0.2	0.1	0.5	2.0	1.0	1.24664	0.828419	1.19063
0.8	3.0	0.5	0.2	0.2	0.1	0.5	2.0	1.0	1.24664	1.023721	1.20708
0.8	3.0	1.0	0.2	0.2	0.1	0.5	2.0	1.0	1.24664	1.181901	1.21687
0.8	3.0	0.5	0.0	0.2	0.1	0.5	2.0	1.0	1.24664	0.977921	1.20122
0.8	3.0	0.5	1.0	0.2	0.1	0.5	2.0	1.0	1.24664	1.161371	1.21987
0.8	3.0	0.5	2.0	0.2	0.1	0.5	2.0	1.0	1.24664	1.282780	1.22721
0.8	3.0	0.5	0.2	0.0	0.1	0.5	2.0	1.0	1.24664	1.121350	1.20399
0.8	3.0	0.5	0.2	0.5	0.1	0.5	2.0	1.0	1.24664	0.905632	1.21163
0.8	3.0	0.5	0.2	1.0	0.1	0.5	2.0	1.0	1.24664	0.759915	1.21905
0.8	3.0	0.5	0.2	0.2	0.0	0.5	2.0	1.0	1.24664	1.044761	1.24855
0.8	3.0	0.5	0.2	0.2	0.3	0.5	2.0	1.0	1.24664	0.982011	1.12713
0.8	3.0	0.5	0.2	0.2	0.5	0.5	2.0	1.0	1.24664	0.941321	1.05104
0.8	3.0	0.5	0.2	0.2	0.1	0.1	2.0	1.0	1.24664	1.256421	1.00359
0.8	3.0	0.5	0.2	0.2	0.1	0.3	2.0	1.0	1.24664	1.133360	1.17306
0.8	3.0	0.5	0.2	0.2	0.1	0.6	2.0	1.0	1.24664	0.973615	1.21561
0.8	3.0	0.5	0.2	0.2	0.1	0.5	1.5	1.0	1.24664	0.939186	1.00666
0.8	3.0	0.5	0.2	0.2	0.1	0.5	2.0	1.0	1.24664	1.023721	1.20708
0.8	3.0	0.5	0.2	0.2	0.1	0.5	3.0	1.0	1.24664	1.097102	1.54359
0.8	3.0	0.5	0.2	0.2	0.1	0.5	2.0	0.5	1.24664	1.089631	0.76433
0.8	3.0	0.5	0.2	0.2	0.1	0.5	2.0	1.0	1.24664	1.023721	1.20708
0.8	3.0	0.5	0.2	0.2	0.1	0.5	2.0	2.0	1.24664	0.965694	1.82509

6. Main Points

In this article, we looked into the problem of boundary layer Carreau nanofluid flow across an impermeable nonlinearly stretching sheet. Analysis of heat and mass transport is modelled under the conditions of thermal radiation, variable heat flux, and viscous dissipation. We employ the shooting approach to address the problem because the emergent system regulating the suggested model was highly nonlinear, forcing us to use numerical technique. Comparison of the skin friction values taken into account shows that the results show good accuracy. Below is a list of the main findings of this analysis:

1. Skin friction coefficient, heat transfer rate, and mass transfer rate are all improved by raising the values of the power law index, while higher values of Weissenberg number behave the reverse tendency.
2. By raising the Lewis number and the Brownian motion parameter, the temperature profile grows and the concentration profile declines.
3. The enhancement of heat transfer and nanoparticle diffusion is caused by the presence of thermal radiation and the variable conductivity of the nanofluid.
4. The local Nusselt and Sherwood numbers are suppressed by raising Prandtl number values.

5. Through the flow of nanofluids, the thermal conductivity parameter acts as a controlling factor of the cooling process.
6. A higher Eckert number along with heat flux greatly raises the temperature and only slightly raises the concentration level.
7. Thermal radiation causes the temperature of the nanofluid to rise away from the sheet, whereas the opposite tendency is seen along the sheet.
8. The Brownian motion parameter and the thermophoresis parameter have qualitatively reciprocal effects on the concentration profile.
9. Future work will build on this research by examining mass flux and how it influences flow through porous medium.

Funding: This research received no external funding.

Institutional Review Board Statement: Not applicable.

Informed Consent Statement: Not applicable.

Data Availability Statement: Not applicable.

Acknowledgments: The author wish to express his sincere thanks to the honorable referees for their valuable comments and suggestions to improve the quality of the paper.

Conflicts of Interest: The author declares no conflict of interest.

References

1. Crane, L.J. Flow past a stretching plate. *Z. Angew. Math. Phys.* **1970**, *2*, 645–647. [CrossRef]
2. Rajagopal, K.R.; Na, T.Y.; Gupta, A.S. Flow of a viscoelastic fluid over a stretching sheet. *Rheol. Acta* **1984**, *23*, 213–215. [CrossRef]
3. Hassanien, I.A.; Abdullah, A.A.; Gorla, R.S.R. Flow and heat transfer in a power-law fluid over a nonisothermal stretching sheet. *Math. Comput. Model.* **1998**, *28*, 105–116. [CrossRef]
4. Megahed, A.M. Variable viscosity and slip velocity effects on the flow and heat transfer of a power-law fluid over a non-linearly stretching surface with heat flux and thermal radiation. *Rheol. Acta* **2012**, *51*, 841–874. [CrossRef]
5. Khan, M.; Shahzad, A. On boundary layer flow of a Sisko fluid over a stretching sheet. *Quaest. Math.* **2013**, *36*, 137–151. [CrossRef]
6. Megahed, A.M. Flow and heat transfer of non-Newtonian Sisko fluid past a nonlinearly stretching sheet with heat generation and viscous dissipation. *J. Braz. Soc. Mech. Sci. Eng.* **2018**, *40*, 492. [CrossRef]
7. Hayat, T.; Abbas, Z.; Sajid, M. MHD stagnation-point flow of an upper-convected Maxwell fluid over a stretching surface. *Chaos Solitons Fractals* **2009**, *39*, 840–848. [CrossRef]
8. Mahmoud, M.A.A. The effects of variable fluid properties on MHD Maxwell fluids over a stretching surface in the presence of heat generation/absorption. *Chem. Eng. Commun.* **2011**, *198*, 131–146. [CrossRef]
9. Nadeem, S.; Hussain, S.T.; Lee, C. Flow of a Williamson fluid over a stretching sheet. *Braz. J. Chem. Eng.* **2013**, *30*, 619–625. [CrossRef]
10. Areshi, M.; Alrihieli, H.; Alali, E.; Megahed, A.M. Temperature Distribution in the Flow of a Viscous Incompressible Non-Newtonian Williamson Nanofluid Saturated by Gyrotactic Microorganisms. *Mathematics* **2022**, *10*, 1256. [CrossRef]
11. Mohammadein, A.A.; Gorla, R.S.R. Heat transfer in a micropolar fluid over a stretching sheet with viscous dissipation and internal heat generation. *Int. J. Numer. Methods Heat Fluid Flow* **2001**, *11*, 50–58. [CrossRef]
12. Turkyilmazoglu, M. Flow of a micropolar fluid due to a porous stretching sheet and heat transfer. *Int. J. Non-Linear Mech.* **2016**, *83*, 59–64. [CrossRef]
13. Carreau, P.J. Rheological equations from molecular network theories. *Trans. Soc. Rheol.* **1972**, *16*, 99–127. [CrossRef]
14. Khan, M.; Hashim; Hussain, M.; Azam, M. Magnetohydrodynamic flow of Carreau fluid over a convectively heated surface in the presence of non-linear radiation. *J. Magn. Magn. Mater.* **2016**, *412*, 63–68. [CrossRef]
15. Khan, M.; Azam, M. Unsteady boundary layer flow of Carreau fluid over a permeable stretching surface. *Results Phys.* **2016**, *6*, 1168–1174. [CrossRef]
16. Machireddy, G.R.; Naramgari, S. Heat and mass transfer in radiative MHD Carreau fluid with cross diffusion. *Ain Shams Eng. J.* **2018**, *9*, 1189–1204. [CrossRef]
17. Kumar, K.G.; Gireesha, B.J.; Rudraswamy, N.G.; Manjunatha, S. Radiative heat transfers of Carreau fluid flow over a stretching sheet with fluid particle suspension and temperature jump. *Results Phys.* **2017**, *7*, 3976–3983. [CrossRef]
18. Hayat, T.; Ullah, I.; Ahmad, B.; Alsaedi, A. Radiative flow of Carreau liquid in presence of Newtonian heating and chemical reaction. *Results Phys.* **2017**, *7*, 715–722. [CrossRef]
19. Choi, U.S. Enhancing thermal conductivity of fluids with nanoparticles. *ASME FED* **1995**, *231*, 99–103.
20. Buongiorno, J. Convective transport in nanofluids. *ASME J. Heat Mass Transf.* **2006**, *128*, 240–250. [CrossRef]
21. Khan, M.; Azam, M.; Alshomrani, A.S. On unsteady heat and mass transfer in Carreau nanofluid flow over expanding or contracting cylinder with convective surface conditions. *J. Mol. Liq.* **2017**, *231*, 474–484. [CrossRef]

22. Azam, M.; Khan, M.; Alshomrani, A.S. Unsteady radiative stagnation point flow of MHD Carreau nanofluid over expanding/contracting cylinder. *Int. J. Mech. Sci.* **2017**, *130*, 64–73. [CrossRef]
23. Khan, M.; Azam, M.; Munir, A. On unsteady Falkner-Skan flow of MHD Carreau nanofluid past a static/moving wedge with convective surface condition. *J. Mol. Liq.* **2017**, *230*, 48–58. [CrossRef]
24. Azam, M.; Khan, M.; Alshomrani, A.S. Effects of magnetic field and partial slip on unsteady axisymmetric flow of Carreau nanofluid over a radially stretching surface. *Results Phys.* **2017**, *7*, 2671–2682. [CrossRef]
25. Mohamed, R.E.; Kasse, L.M.; Taseer, M.; Mohsen, S. Numerical treatment for Carreau nanofluid flow over a porous nonlinear stretching surface. *Results Phys.* **2018**, *8*, 1185–1193.
26. Hayat, T.; Qayyum, S.; Alsaedi, A.; Shafiq, A. Theoretical aspects of Brownian motion and thermophoresis on nonlinear convective flow of magneto Carreau nanofluid with Newtonian conditions. *Results Phys.* **2018**, *10*, 521–528. [CrossRef]
27. Megahed, A.M. Carreau fluid flow due to nonlinearly stretching sheet with thermal radiation, heat flux, and variable conductivity. *Appl. Math. Mech.* **2019**, *40*, 1615–1624. [CrossRef]
28. Megahed, A.M. Improvement of heat transfer mechanism through a Maxwell fluid flow over a stretching sheet embedded in a porous medium and convectively heated. *Math. Comput. Simul.* **2021**, *187*, 97–109. [CrossRef]
29. Cortell, R. Effects of viscous dissipation and radiation on the thermal boundary layer over a non-linearly stretching sheet. *Phys. Lett. A* **2008**, *372*, 631–636. [CrossRef]
30. Khan, M. Hashim Boundary layer flow and heat transfer to Carreau fluid over a nonlinear stretching sheet. *AIP Adv.* **2015**, *5*, 107203. [CrossRef]
31. Alrihieli, H.; Areshi, M.; Alali, E.; Megahed, A.M. MHD dissipative Williamson nanofluid flow with chemical reaction due to a slippery elastic sheet which was contained within a porous medium. *Micromachines* **2022**, *13*, 1879. [CrossRef]